p70 S6 kinase in the control of actin cytoskeleton dynamics and directed migration of ovarian cancer cells

C K M Ip[1], A N Y Cheung[2], H Y S Ngan[3], and A S T Wong[1]

[1]School of Biological Sciences, [2]Department of Pathology, and [3]Department of Obstetrics and Gynecology, University of Hong Kong, Pokfulam Road, Hong Kong

Correspondence: Dr AST Wong, School of Biological Sciences, University of Hong Kong, 4S-14 Kadoorie Biological Sciences Building, Pokfulam Road, Hong Kong. Email: awong1@hku.hk.

Running title: $p70^{S6K}$ signaling to the actin cytoskeleton

Keywords: p70 S6 kinase; ovarian cancer; actin; Rac1; Cdc42

The authors declare no conflict of interest.

Word count: 4418

Abstract

Ovarian cancer is highly metastatic with a poor prognosis. The serine/threonine kinase, p70 S6 kinase ($p70^{S6K}$), which is a downstream effector of phosphatidylinositol 3-kinase/Akt pathway, is frequently activated in ovarian cancer. Here, we show that $p70^{S6K}$ is a critical regulator of the actin cytoskeleton in the acquisition of the metastatic phenotype. This regulation is through two important activities: $p70^{S6K}$ acts as an actin filament cross-linking protein and as a Rho family GTPase-activating protein. Ectopic expression of constitutively active $p70^{S6K}$ in ovarian cancer cells induced a marked reorganization of the actin cytoskeleton and promoted directional cell migration. Using cosedimentation and differential sedimentation assays, $p70^{S6K}$ was found to directly bind to and cross-link actin filaments. Immunofluorescence studies showed $p70^{S6K}$ colocalized with cytochalasin D-sensitive actin at the leading edge of motile cells. $p70^{S6K}$ did not affect the kinetics of spontaneous actin polymerization, but could stabilize actin filaments by the inhibition of cofilin-induced actin depolymerization. In addition, we showed that $p70^{S6K}$ stimulated the rapid activation of both Rac1 and Cdc42, and their downstream effector p21-activated kinase (PAK1), but not RhoA. Depletion of $p70^{S6K}$ expression or inhibition of its activity resulted in significant inhibition of actin cytoskeleton reorganization and reduced migration, with a concomitant reduction in Rac1, Cdc42, and

PAK1 activation, confirming that the effect was $p70^{S6K}$ specific. Similarly, the actin cytoskeleton reorganization/migratory phenotype could be reversed by expression of dominant negative Rac1 and Cdc42, or inhibition of PAK1. These results reveal a new direction for understanding the oncogenic roles of $p70^{S6K}$ in tumor progression.

Introduction

Ovarian cancer is the leading cause of death among all gynecological malignancies (Jemal *et al.*, 2009). Nearly 70% of patients are diagnosed at the advanced stages, which have already metastasized cancer cells that detach from the primary tumor, spread throughout the peritoneum forming malignant ascites, adhere to and eventually invade organs within the peritoneal cavity. No effective therapy for advanced or metastatic ovarian carcinoma is currently available, and the poor 5-year survival rate is <25%. Thus, it is important to better understand the mechanisms by which these cells acquire metastatic properties and to identify new potential molecular targets.

p70 S6 kinase ($p70^{S6K}$) is a downstream effector of the phosphatidylinositol 3-kinase (PI3K)/Akt pathway, which is frequently activated in human ovarian cancer (Shayesteh *et al.*, 1999; Philp *et al.*, 2001; Altomare *et al.,* 2004). $p70^{S6K}$ is also well known to be activated by cytokines and growth factors, including epidermal growth factor and hepatocyte growth factor (HGF), which are potent inducers of $p70^{S6K}$ in ovarian cancer (Liu *et al.*, 2006; Zhou and Wong, 2006). Constitutive activation of $p70^{S6K}$ is significantly more prevalent in malignant ovarian tumors than in benign lesions (Castellvi *et al.*, 2006). Recently, in addition to its well-established role in regulating proliferation and cell

survival, we show for the first time that $p70^{S6K}$ may be involved in other aspects of ovarian cancer progression, such as metastasis (Wong *et al.*, 2004; Zhou and Wong, 2006; Pon *et al.*, 2008). However, the role of $p70^{S6K}$ in cell migration, which is a key process directly linked to cancer invasion and metastasis, has not been established, and the mechanism by which $p70^{S6K}$ contributes to this process is also unknown.

Reorganization of the actin cytoskeleton is both essential and central for cell migration (Pantaloni *et al.*, 2001). Motile cancer cells must assemble and disassemble the actin filaments at their leading edges as they move forward. Thus, deregulation of the expression or properties of actin-binding proteins that regulate the polymerization/depolymerization of actin into filaments, and cross-linking of these into bundles could influence metastasis (Pawlak and Helfman, 2001). The Rho family of small GTPases, in particular Rac1, Cdc42, and RhoA, are molecular switches that control the organization and dynamics of the actin cytoskeleton (Ridley *et al*., 2003; Raftopoulou and Hall, 2004): Rac1 regulates the formation of membrane ruffles (lamellipodia), Cdc42 triggers membrane projections (filopodia), and RhoA regulates stress fiber and focal adhesions. In addition, Rac1 is essential for forward cellular movement and Cdc42 is required for dictating the direction of migration.

In the present study, we show for the first time a role for $p70^{S6K}$ in the directed migration of human ovarian cancer cells. We also provide mechanistic insights suggesting that this tumorigenic activity is associated with the ability of $p70^{S6K}$ to directly and indirectly reorganize the actin cytoskeleton through its actin filament cross-linking and Rac1/Cdc42-activating activities.

Results

$p70^{S6K}$ activation causes reorganization of the actin cytoskeleton

The rapid reorganization of the actin cytoskeleton is a critical early event in cell migration (Pantaloni *et al.*, 2001). To address if $p70^{S6K}$ modifies actin organization in the cell, we tested the effects of constitutively active $p70^{S6K}$ activation on the actin cytoskeleton in CaOV-3 and SKOV-3 ovarian cancer cell lines, which represent advanced human ovarian cancer (Buick *et al.*, 1985). When constitutively active $p70^{S6K}$ ($\Delta N_{54}\Delta C_{104}$ and D_3E-E_{398}) was ectopically expressed, there was a marked difference in both cellular morphology and actin cytoskeleton architecture. $\Delta N_{54}\Delta C_{104}$- and D_3E-E_{398}-transfected cells had prominent actin-rich projections in the form of lamellipodia, actin microspikes, and filopodia which were absent in the untransfected cells (Figure 1a). Even after 24 h, there were no protrusions present in the control cells (data not shown).

To further demonstrate the effect of $p70^{S6K}$ in altering the actin cytoskeleton, we utilized a siRNA specifically engineered towards $p70^{S6K}$. In these studies, HGF was used to activate endogenous $p70^{S6K}$, because HGF is highly expressed in ovarian cancer ascites inducing migration of cultured ovarian cancer cells (Sowter *et al.*, 1999). Overexpression of the HGF receptor Met is associated with ovarian cancer progression and high Met expression correlates with poor survival (Sawada *et al.*, 2007). The $p70^{S6K}$-specific siRNA, but not the nonspecific siRNA, was effective in depleting $p70^{S6K}$ expression as confirmed by Western blotting (Figure 1b, inset). We observed that $p70^{S6K}$ siRNA treated ovarian cancer cells resulted in dramatically reduced HGF-stimulated actin reorganization and reduced formation of membrane protrusions (Figure 1b). A second $p70^{S6K}$ specific siRNA was also used, and comparable results were obtained, which confirms that $p70^{S6K}$ was responsible for this effect (data not shown). In contrast, nonspecific siRNA did not obviously alter the pattern of actin distribution. Similar results were observed in cells treated with rapamycin, which is a small molecule inhibitor of $p70^{S6K}$ kinase activity (Figure 1b). Together, these data show that $p70^{S6K}$ activation plays a critical role in the reorganization of actin cytoskeleton.

$p70^{S6K}$ is required for directional migration

Because directed cell migration is a prerequisite of metastasis, we assessed the role of $p70^{S6K}$ on cell migration using scrape wounding assays combined with Golgi tracking (Ridley *et al.*, 2003). We found that $p70^{S6K}$ siRNA treated cells migrated less efficiently than the control nonspecific siRNA treated cells, and also exhibited significantly reduced directional persistence (98% inhibition of a polarized orientation of the Golgi apparatus) in the presence of HGF (Figure 2a). The role of $p70^{S6K}$ in directional cell migration was further evaluated by measuring the movement of the cells towards a chemotactic stimulus using Boyden chamber assays. Activation of $p70^{S6K}$ significantly promoted a motile phenotype, as detected by a 2.8-fold increase in cell motility compared with control cells (Figure 2b). In contrast, the HGF-enhanced migration was effectively suppressed by siRNA-mediated depletion of $p70^{S6K}$ to near basal levels (Figure 2b). Under these conditions, and consistent with previous observation (Corps *et al.*, 1997), HGF did not cause significant alterations of cell proliferation (Supplementary Figure 1). We also found no effect of constitutively active $p70^{S6K}$ on cell proliferation (Supplementary Figure 1), indicating that the increase in cell migration was not because of a proliferative effect.

$p70^{S6K}$ binds directly to actin

To begin to understand the mechanism of $p70^{S6K}$ involvement in signaling the actin cytoskeleton, we used a cosedimentation assay to investigate if $p70^{S6K}$ binds actin filament *in vitro*. As shown in Figure 3a, endogenous active $p70^{S6K}$ readily cosedimented with actin. Moreover, stimulation of HGF increased the amount of phospho-$p70^{S6K}$ sedimented in the actin pellet, suggesting that activated $p70^{S6K}$ can more capably associate with actin.

We further asked whether the interaction of $p70^{S6K}$ with actin by direct interaction or is mediated by other actin-binding proteins. To test this, an *in vitro* actin binding assay was performed using highly purified active $p70^{S6K}$. Figure 3b shows that the purified $p70^{S6K}$ could be readily coprecipitated with actin in a concentration-dependent manner. $p70^{S6K}$ alone did not pellet, indicating that the pelleting is due to binding to F-actin (Figure 3c). The fact that no other proteins were involved indicates a direct association between $p70^{S6K}$ and actin.

This interaction was additionally verified by colocalization analysis using immunofluorescence microscopy. While phospho-$p70^{S6K}$ was located diffusely through the control cells, it was translocated to and, interestingly, concentrated in lamellipodia, actin microspikes, and filopodia where it was extensively colocalized with actin upon

stimulation with HGF (Figure 3d, left). We further confirmed our results using myc-tagged D_3E-E_{398}. We found that D_3E-E_{398} was colocalized with actin at membrane protrusions of lamellipodia and filopodia (Figure 3d, right). These changes were inhibited by disruption of actin filaments by cytochalasin D treatment (Figure 3e), indicating that the binding of $p70^{S6K}$ to the cytoskeleton is mediated by actin. Similar experiments with SKOV-3 revealed $p70^{S6K}$-actin interaction indistinguishable from those in CaOV-3 (Supplementary Figures 2a and b).

$p70^{S6K}$ cross-links and stabilizes F-actin

To further establish the role that $p70^{S6K}$ plays in the actin cytoskeleton, we repeated the cosedimentation assay, this time using a low-speed (14,000 *g*) to pellet the bundled or cross-linked actin filaments, while the free actin filaments remain in the supernatant. HGF caused the majority of actin filaments to pellet with endogenous phospho-$p70^{S6K}$ during low speed centrifugation, suggesting that active $p70^{S6K}$ is cross-linking individual filaments into actin bundles (Figure 4a and Supplementary Figure 2c). This was also examined using purified proteins: F-actin was detected in the supernatant when $p70^{S6K}$ was absent, but in the pellet when $p70^{S6K}$ was present, with an increasing shift between free to bundled actin with increasing molar concentrations of $p70^{S6K}$ (Figure 4b). Light

scattering assay was used to monitor the kinetics of $p70^{S6K}$-induced actin bundle formation. Light scattering increased rapidly and reached almost steady state within 5 min, indicating that $p70^{S6K}$ quickly binds to actin filaments. Light scattering also increased with increasing concentrations of $p70^{S6K}$, suggesting that more actin bundles were formed (Figure 4c). We also used electron microscopy to visualize the F-actin bundling. In the absence of $p70^{S6K}$, actin filaments formed a uniform meshwork of fine filaments but did not show bundling. In contrast, robust multifilament bundles were clearly seen (Figure 4d). These closely apposed bundles were often slightly curved, suggesting flexible cross-linking.

The possibility of a physical interaction between $p70^{S6K}$ and actin suggests that $p70^{S6K}$ may affect the kinetics of actin polymerization. $p70^{S6K}$ did not change the rate or the extent of polymerization, suggesting that unlike other common activities of these proteins, actin polymerization is not a generic property of $p70^{S6K}$ (Figure 5a). On the other hand, $p70^{S6K}$ significantly decreased the rate and extent of actin filament depolymerization (Figure 5b). Fluorescence from pyrene-labeled F-actin decreased rapidly after addition of cofilin. This decrease in fluorescence was largely reduced with F-actin pre-incubated with purified $p70^{S6K}$, suggesting $p70^{S6K}$ prevented depolyermization of F-actin induced by cofilin. These results indicate that in addition to

cross-linking of F-actin, $p70^{S6K}$ also stabilizes filaments.

$p70^{S6K}$ induces activation of Rac1 and Cdc42

We next sought to determine the molecular mechanism by which $p70^{S6K}$ regulates actin organization. Three members of the Rho family GTPases, Rac1, Cdc42, and RhoA, are best known for their effects on the actin cytoskeleton (Hall, 1998). In fibroblasts, it has been shown that Rho GTPases have the potential to regulate $p70^{S6K}$, suggesting that $p70^{S6K}$ may be a downstream effector (Berven *et al.*, 2004; Chou and Blenis, 1996). However, transfection with dominant negative Rac (N17Rac1), Cdc42 (N17Cdc42), or Rho (N19RhoA) failed to block $p70^{S6K}$ phosphorylation (activation) upon HGF stimulation in CaOV-3 cells (Supplementary Figure 3a). Similarly, ectopic expression of constitutively active Rac (L61Rac1), Cdc42 (V12Cdc42), and Rho (V14RhoA) were unable to activate $p70^{S6K}$ (Supplementary Figure 3b).

Because its roles in actin cytoskeleton reorganization similar to the activation of Rho GTPases, we investigated if $p70^{S6K}$ might act upstream of Rho GTPases. To explore this possibility, we tested the effects of $p70^{S6K}$ on Rac1, Cdc42, and RhoA activation using a pull-down assay that specifically recognizes the active GTP-bound form. As shown in Figure 6a, HGF rapidly increased activities of Rac1 and Cdc42 within 15-30 min, and

Rac1 and Cdc42 activation also coincided with the activation of $p70^{S6K}$. In addition, expression of active $p70^{S6K}$ potently stimulated the activation of both Rac1 and Cdc42, whereas it did not have an effect on RhoA (Figure 6a), which is consistent with its enrichment in lamellipodia and filopodia (Fig. 1). To further elucidate the activation of Rac1 and Cdc42 was $p70^{S6K}$ specific, we used siRNA. In cells transfected with $p70^{S6K}$ siRNA, but not control siRNA, the ability of HGF to activate Rac1 and Cdc42 was abrogated (90% inhibition) (Figure 6b). Similarly, HGF-dependent activation of Rac1 and Cdc42 was also blocked in the presence of rapamycin (80% inhibition) (Figure 6c). Similar results were obtained with SKOV-3 cells (Supplementary Figures 2d and e). These results identify $p70^{S6K}$ as an upstream regulator of Rac1 and Cdc42.

Rac1 and Cdc42 are mediators of $p70^{S6K}$-regulated actin reorganization

To investigate if $p70^{S6K}$ signals the actin cytoskeleton via Rac1 and Cdc42, we examined the actin cytoskeleton of cells cotransfected with myc-tagged dominant negative mutants of Rac1 and Cdc42 and GFP-tagged constitutively active $p70^{S6K}$. Expression of N17Rac1 or N17Cdc42 was shown to clearly inhibit the $p70^{S6K}$-induced restructuring of the actin cytoskeleton (Figure 7a). Conversely, constitutively active Rac1 and Cdc42 enhanced cell spreading and caused reorganization of the actin cytoskeleton (lamellipodia/filopodia) to

levels similar to those observed in $p70^{S6K}$-expressing cells (Figure 7b). To explore the relationship between $p70^{S6K}$ and Rac1/Cdc42, we investigated a possible interaction between these two proteins. Figure 7c demonstrates a colocalization of phospho-$p70^{S6K}$ with Rac1/Cdc42 in HGF-stimulated cells, but not in control cells.

The p21-activated kinase (PAK1) is a well-characterized effector of both Rac1 and Cdc42 and is essential for regulating leading edge actin dynamics (Dummler *et al.*, 2009). Our finding that the activities of both Rac1 and Cdc42 are important in $p70^{S6K}$-mediated actin cytoskeleton reorganization prompted us to assess the role of PAK. We found that $p70^{S6K}$ was able to stimulate the phosphorylation of PAK1, and that stimulation was lost in HGF-treated cells transfected with the $p70^{S6K}$ siRNA (Figure 8a). Knocking down PAK1 impaired the pronounced lamellipodia/filopodia phenotype in response to transfection of constitutively active $p70^{S6K}$ (Figure 8b). These cells also displayed a loss of the motile phenotype (Figure 8c). Another PAK1 siRNA also showed comparable results (Figure 8), whereas a nonspecific siRNA had no effect. These data demonstrate an essential role of Rac1/Cdc42/PAK1 signaling in actin cytoskeleton reorganization and the regulation of ovarian cancer cell motility downstream of $p70^{S6K}$.

Discussion

In this study, we have successfully identified $p70^{S6K}$ as a novel regulator of the actin cytoskeleton and found that it is pivotal for the directed migration of ovarian cancer cells. We show that two important properties underlie this function of $p70^{S6K}$, namely actin cross-linking and Rac1 and Cdc42 activation (Figure 9). Several aspects of this function are worth highlighting. We showed for the first time that $p70^{S6K}$ was able to bind to F-actin with no other proteins involved, indicating direct binding of $p70^{S6K}$ to F-actin. The finding that $p70^{S6K}$ F-actin structures were cytochalasin D sensitive emphasizes the possibility that *in vitro* interactions of $p70^{S6K}$ with F-actin may represent direct interactions of $p70^{S6K}$ with actin filaments *in vivo*. Moreover, the binding of $p70^{S6K}$ to F-actin was more potent in the presence of phosphorylation than in its absence, suggesting a dynamic regulation of $p70^{S6K}$ association with the cytoskeleton and reinforces the notion that actin reorganization and cell migration are finely tuned events. This also implies that the actin-binding domain in $p70^{S6K}$ may normally be hidden when this protein is in an inactive conformation.

An intriguing aspect concerns the biological function of such an interaction. The finding that $p70^{S6K}$ both cross-links and stabilizes actin filaments suggests a role for $p70^{S6K}$ in

regulating actin dynamics. Several key actin-binding proteins such as α-actinin, fimbrin, and fascin also function to regulate actin bundling (Holmes *et al.*, 1976; Hanein *et al.*, 1997). Because $p70^{S6K}$ has a well-established role in protein synthesis, this interaction may also have significance in synthesizing local proteins important for propagating the migratory response. For example, β-actin mRNA has been shown to localize to the leading lamella and its active translation there is important for cell migration (Kislauskis *et al.*, 1994; Latham *et al.*, 1994).

The Rho family of GTPases are critical regulators of actin reorganization. Studies using fibroblasts have suggested that Rho GTPases and $p70^{S6K}$ may reside on a common signaling pathway, and indeed these studies indicate that Rho GTPases are upstream activators of $p70^{S6K}$ (Chou and Blenis, 1996; Berven *et al.*, 2004). In contrast to the above data, we found that, in ovarian cancer cells, Rac1 and Cdc42 did not regulate $p70^{S6K}$ function. Rather, Rac1 and Cdc42 are downstream effectors of $p70^{S6K}$. One possible explanation is that this action may be cell-type dependent. Clearly, epithelial cells and fibroblasts display distinct architecture of the actin cytoskeleton. Rac has been demonstrated to evoke different responses depending on the cell type (Takaishi *et al.*, 1997; Sander *et al.*, 1998). Another possibility, and one that is supported by the findings

reported here, is that it may be related to the different functions of $p70^{S6K}$. It is interesting to note that activation of $p70^{S6K}$ by Rac1 and Cdc42 appears to be independent of the ability of these Rho GTPases to regulate the cytoskeleton (Chou and Blenis, 1996). In contrast, we show that Rac and Cdc42 mediate signaling from $p70^{S6K}$ is related to cytoskeletal reorganization, which Rac/Cdc42 are known to function during this process (Hall, 1998).

The increase in Rac1 and Cdc42 activities in response to $p70^{S6K}$ sheds new light on the biochemical mechanism of $p70^{S6K}$ function and identifies $p70^{S6K}$ as a novel, important regulator of Rho GTPases. How does $p70^{S6K}$ control the function of Rac1/Cdc42? Guanine nucleotide exchange factors (GEFs) are known to activate Rho GTPases by regulating the exchange of GDP for GTP. The Dbl homology-Pleckstrin homology (DH-PH) motif, present in many of proteins such as GEFs, is responsible for activation of Rac1 and Cdc42 (Erickson and Cerione, 2004). However, $p70^{S6K}$ does not contain a DH-PH domain or other motifs that may elicit GEF activity. Given the fact that TOR proteins regulate Rho GTPase activity via a GTP exchange factor, ROM2, in yeast (Schmidt *et al.*, 1997), it is possible that an additional protein, such as GEF, may be necessary for $p70^{S6K}$-mediated Rac1/Cdc42 activation. We also showed an essential role

for PAK1 in Rac1/Cdc42-mediated actin cytoskeleton reorganization downstream of $p70^{S6K}$. This finding is intriguing because PAK1 has been observed as the predominant isoform that is frequently activated in ovarian tumors and appears to be associated with tumor aggressiveness (Schraml *et al.*, 2003; Siu *et al.*, 2009). Once activated, PAK1 may locally affect the actin organization via direct phosphorylation of key signaling targets. For example, PAK1 phosphorylates and inactivates the actin-depolymerizing protein cofilin leading to actin filament stabilization (Dummler *et al.*, 2009). The observation that $p70^{S6K}$ can also physically cross-link and stabilize the filaments suggests that multiple mechanisms that control stable actin structures are likely to be regulated by $p70^{S6K}$ and gives support that this kinase is a critical regulator of the actin cytoskeleton.

The ability of $p70^{S6K}$ to modulate dynamics of the actin cytoskeleton suggests that many oncogenic pathways could govern tumor invasion/metastasis by modulating $p70^{S6K}$. $p70^{S6K}$ activation did not cause significant alteration to the actin cytoskeleton of normal OSE (Supplementary Figure 4), which suggests that the effect may be specific to ovarian cancer cells. It also complements our previous finding and other studies that showed a differential effect on OSE (Wong *et al*., 2004; Theriault *et al.*, 2007) and the acquisition of a motile, fibroblast-like phenotype in OSE may be regulated independent of PI3K and

is a slow process (Ahmed *et al.*, 2006). We and others have described the frequent activation of $p70^{S6K}$ in ovarian cancer cells than in normal OSE, suggesting a critical role for $p70^{S6K}$ in ovarian cancer development and progression (Wong *et al.*, 2004; Castellvi *et al.*, 2006; Pon *et al.*, 2008). The observation that $p70^{S6K}$ was highly expressed and activated in high-grade, poorly differentiated ovarian carcinomas further suggests that $p70^{S6K}$ may be associated with tumor aggressiveness. Possible involvement of $p70^{S6K}$ in the regulation of cell migration is also particularly intriguing because the malignant phenotypes from patients with advanced breast cancer, colon cancer, and hepatocellular carcinoma are also correlated with increased activation of $p70^{S6K}$ (Filonenko *et al.*, 2004; Sahin *et al.*, 2004; Nozawa *et al.*, 2007). We found that active $p70^{S6K}$ was able to bind and cross-link actin filaments and regulate actin organization in HepG2 liver cancer cells (Supplementary Figure 5), further suggesting that the cytoskeletal function of $p70^{S6K}$ we propose here may have broad implications for other tumor cell types as well.

In summary, the present study reveals the novel identification of the localization and function of $p70^{S6K}$ in the actin cytoskeleton. The results show that $p70^{S6K}$ has pivotal roles in regulating metastatic progression, and opens new areas for further investigation. Such findings greatly advance our understanding of the role of $p70^{S6K}$ in oncogenesis and

highlight that usefulness of targeting $p70^{S6K}$ to impede metastasis in ovarian cancer.

Materials and methods

Cells and cell culture

Institutional approval for experimentation with human tissues was obtained prior to this study. OSE-529, OSE-545, and OSE-547 were obtained from ovaries at laparoscopy from women having surgery for non-malignant gynecologic diseases. The human ovarian carcinoma cell lines CaOV-3 and SKOV-3 were gifts from Dr. N. Auersperg (University of British Columbia, Vancouver, B. C., Canada). Cells were cultured in media 199:MCDB105 supplemented with 10% fetal bovine serum (FBS) for OSE and 5% FBS for ovarian cancer cell lines. HepG2 human liver cancer cell line was maintained in DME containing 5% FBS. Cells were grown in humidified atmosphere of 5% CO_2 at 37^{o}C.

DNA constructs and transfection

N17Rac1 and L61Rac1 constructs were kindly provided by Dr. A. Hall (Memorial Sloan-Kettering Cancer Center, New York, NY) (Olson *et al.,* 1995). N17Cdc42, V12Cdc42, N19RhoA, and V14RhoA were obtained from UMR cDNA Resource Center (Missouri, MO). The myc-tagged constitutively active $p70^{S6K}$ ($\Delta N_{54}\Delta C_{104}$ and D_3E-E_{398}) were gifts from Dr. G. Thomas (Genome Research Institute, University of Cincinnati, Cincinnati, OH) (Jefferies *et al.*, 1997). GFP-tagged D_3E-E_{398} was constructed by

subcloning into pEGFP vector (Clontech). To express cDNA constructs, cells were transiently transfected with 1 μg of plasmid DNA per well in 6-well plates using Lipofectamine 2000 reagent (Invitrogen).

Small interfering RNA

$p70^{S6K}$-specific siRNA (#3, 5'-GACAAAAUCCUCAAAUGUA-3'; #4, 5'-GCAGGAGUGUUUGACAUAG-3') (Pon *et al.*, 2008), PAK1-specific siRNA (#1, 5'-CAUCAAAUAUCACUAAGUC-3'; #2, 5'-CAACAAAGAACAAUCACUA-3'), and a nonspecific duplex oligo (5'-GGCTACGTCCAGGAGCGCA-3') as a negative control were purchased from Dharmacon (Lafayette, CO). Cells were transfected overnight with 20 nM of siRNA using siLectFect (Bio-Rad) following the manufacturer's instruction.

Western blotting

Equal amounts of cell lysates were resolved by SDS-PAGE. The samples were incubated overnight at $4^{o}C$ with the following primary antibodies: anti-c-myc (clone 9E10) (1:1,500), anti-phospho-$p70^{S6K}$ (Thr389) (1:1,000), anti-$p70^{S6K}$ (1:1,000), anti-phospho-S6 (Ser235/236) (1:1,000), anti-S6 (1:1,000), anti-phospho-PAK1 (Ser144)/PAK2 (Ser141) (1:1,000), anti-PAK1 (1:1,000), (Cell Signaling), anti-Rac1

(clone 23A8) (1:1,000), anti-Cdc42 (1:250), anti-RhoA (clone 55) (1:250) (Upstate), and anti-β-actin (1:1,500) (Sigma). Proteins were visualized by enhanced chemiluminescence (Amersham).

Fluorescence microscopy

To detect F-actin, cells were fixed in 4% paraformaldehyde in PBS. Cells were permeabilized with 0.1% Triton X-100, blocked with 5% BSA, and then incubated with Texas red-conjugated phalloidin (4 units/ml; Molecular Probes) for 1 h at room temperature. Images were observed by confocal microscopy using a Leica DMRB. In some cases, cells were treated with 1 μM cytochalasin D (Calbiochem) (known to disrupt actin filaments) for 30 min prior to fixation.

Actin binding assay

Binding of $p70^{S6K}$ to actin was tested in a cosedimentation assay according to the manufacturer's instructions (Cytoskeleton). Briefly, cell lysates were first precleared by centrifugation at 800 *g* for 6 min and then incubated in the presence or absence of polymerized rabbit α-skeletal muscle actin at room temperature for 30 min. The reaction mixtures were centrifuged at 150,000 *g* for 90 min. BSA, which does not bind actin, and

α-actinin, an actin-binding protein, were used as negative and positive controls, respectively. The supernatant and pellet were separated and equal amounts were analyzed by Western blotting using anti-phospho-$p70^{S6K}$ antibody.

To examine whether $p70^{S6K}$ directly interacts with actin, purified recombinant human active $p70^{S6K}$ (R&D Systems) was used. After 1 h incubation at room temperature, actin filaments and bound purified proteins were pelleted by centrifugation at 100,000 *g* for 1 h at 20°C. Equal amounts of the pellet and supernatant were analyzed by SDS-PAGE and Coomassie Blue staining.

Actin cross-linking assay

Precleared cell lysates or purified $p70^{S6K}$ (R&D Systems) was added to 4.5 μM freshly prepared F-actin for 1 h at room temperature, and was then centrifuged at 14,000 *g* for 1 min to sediment bundled F-actin, the linear, unbundled F-actin remains in the supernatant. Equal amounts of the pellet and supernatant were analyzed by SDS-PAGE and the gel was stained with Coomassie Blue.

Light scattering and electron microscopy

Changes in light scattering of unlabeled actin was monitored by 90° light scattering at

405 nm (Perkin Elmer). The change of light scattering was recorded after addition of polymerization buffer to purified $p70^{S6K}$ and G-actin. Electron microscopy was performed on samples after actin polymerization was complete, as monitored by light scattering. Samples were fixed by 0.05% glutaraldehyde, spotted onto carbon-coated formvar grids, and negative stained with 2% uranyl acetate. Images were recorded on a CCD camera with a Philips EM208s transmission electron microscope (Eindhoven, The Netherlands).

Actin polymerization assay

Purified G-actin (2.5 μM, 10% pyrene-labeled) was incubated with purified $p70^{S6K}$ for 30 min, and polymerization was initiated with 0.1 volume of 10x polymerization buffer. To measure cofilin-induced depolymerization, 1 μM polymerized filaments were incubated with purified $p70^{S6K}$ for 30 min, and actin depolymerization was induced by the addition of 1 μM recombinant purified human cofilin (Cytoskeleton). The change in fluorescence was monitored over time with excitation at 355 nm and emission at 405 nm using a Victor X4 plate reader (Perkin Elmer).

Cell polarity and migration analysis

Cells were cultured to confluency and scraped using a pipette tip. Cells at the wound edge with Golgi (anti-GM130, Sigma) polarized to the front-facing 120^{o} sector were scored as positive for polarization. Migration assay was performed using a 24-well Transwell inserts (8 μm pore size; Millipore). Cells (1.5×10^4 per well) were placed in the upper chamber, and 5% serum was placed in the lower chamber as a chemoattractant. The migratory phenotype was determined by counting the cells that had migrated to the lower side of the filter. Results were presented as the mean cell number of five fields ± SD of triplicate experiments.

Rac1, Cdc42, and RhoA activity assay

Pull-down assays were performed to isolate the active GTP-bound form using the Rac1/Cdc42 and RhoA activation assay kits (Upstate) following the manufacturer's instructions. Briefly, 10 μg of agarose conjugated GST-PAK-1 PBD fusion protein were added to the lysate and rotated for 1 h at 4^{o}C. The beads were washed three times, eluted with sample buffer and immunoblotted for either Rac1 or Cdc42. A similar assay, using the Rhoketin Rho binding domain (RBD) as a GST fusion protein, was used to measure RhoA activation. For negative and positive controls, cell extracts were incubated with 1

mM GDP and 100 μM GTPγS, respectively.

Statistical analysis

Data were expressed as mean ± SD. Experiments were performed three times. Statistical significance was evaluated with Student's *t* test. $P < 0.05$ was considered to be significant.

Acknowledgments

We thank Drs N Auersperg, G Thomas, and A Hall for providing cell lines and cDNA constructs. This work was supported by the Research Grant Council grant HKU 7599/05M and the HKU Outstanding Young Research Award (AST Wong).

References

Ahmed N, Maines-Bandiera S, Quinn MA, Unger WG, Dedhar S, Auersperg N (2006) Moleuclar pathways regulating EGF-induced epithelio-mesenchymal transition in human ovarian surface epithelium. *Am J Physiol Cell Physiol* **290:** C1532-1542.

Altomare DA, Wang HQ, Skele KL, De Rienzo A, Klein-Szanto AJ, Godwin AK *et al* (2004). AKT and mTOR phosphorylation is frequently detected in ovarian cancer and can be targeted to disrupt ovarian tumor growth. *Oncogene* **23:** 5853-5857.

Berven LA, Willard FS, Crouch MF (2004). Role of the p70(S6K) pathway in regulating the actin cytoskeleton and cell migration. *Exp Cell Res* **296:** 183-195.

Buick RN, Pullano R, Trent JM (1985) Comparative properties of five human ovarian adenocarcinoma cell lines. *Cancer Res* **45:** 3668-3676.

Castellvi J, Garcia A, Rojo F, Ruiz-Marcellan C, Gil A, Baselga J *et al* (2006). Phosphorylated 4E binding protein 1: A hallmark of cell signaling that correlates with survival in ovarian cancer. *Cancer* **107:** 1801-1811.

Chou MM, Blenis J (1996). The 70 kDa S6 kinase complexes with and is activated by the Rho family G proteins Cdc42 and Rac1. *Cell* **85:** 573-583.

Corps AN, Sowter HM, Smith SK (1997). Hepatocyte growth factor stimulates motility, chemotaxis and mitogenesis in ovarian carcinoma cells expressing high levels of

c-met. *Int J Cancer* **73:** 151-155.

Dummler B, Ohshiro K, Kumar R, Field J (2009). Pak protein kinases and their role in cancer. *Cancer Metastasis Rev* **28:** 51-63.

Erickson JW, Cerione RA (2004). Structural elements, mechanism, and evolutionary convergence of Rho protein-guanine nucleotide exchange factor complexes. *Biochemistry* **43:** 837-842.

Filonenko VV, Tytarenko R, Azatyan SK, Savinskal LO, Gaydar YA, Gout IT *et al* (2004). Immunohistochemical analysis of S6K1 and S6K2 localization in human breast tumors. *Exp Oncol* **26:** 294-299.

Hall A (1998). Rho GTPases and the actin cytoskeleton. *Science* **279:** 509-514.

Hanein D, Matsudaira P, DeRosier DJ (1997). Evidence for a conformational change in actin induced by fimbrin (N375) binding. *J Cell Biol* **139:** 387-396.

Holmes GR, Goll DE, Suzuki A, Robson RM, Stromer MH (1976). Effect of trypsin on rabbit skeletal-muscle alpha-actinin. *Biochim Biophys Acta* **446:** 445-456.

Jefferies HBJ, Fumagalli S, Dennis PB, Reinhard C, Pearson RB, Thomas G (1997). Rapamycin suppresses 5'TOP mRNA translation through inhibition of p70(S6k). *EMBO J* **16:** 3693-3704.

Jemal A, Siegel R, Ward E, Hao YP, Xu JQ, Thun MJ (2009). Cancer Statistics, 2009.

CA-Cancer J Clin **59:** 225-249.

Kislauskis EH, Zhu XC, Singer RH (1994). Sequences responsible for intracellular-localization of beta-actin messenger-RNA also affect cell phenotype. *J Cell Biol* **127:** 441-451.

Latham VM, Kislauskis EH, Singer RH, Ross AF (1994). Beta-actin messenger-RNA localization is regulated by signal-transduction mechanisms. *J Cell Biol* **126:** 1211-1219.

Liu LZ, Hu XW, Xia C, He J, Zhou Q, Shi X *et al* (2006). Reactive oxygen species regulate epidermal growth factor-induced vascular endothelial growth factor and hypoxia-inducible factor-1 alpha expression through activation of AKT and P70S6K1 in human ovarian cancer cells. *Free Radic Biol Med* **41:** 1521-1533.

Nozawa H, Watanabe T, Nagawa H (2007). Phosphorylation of ribosomal p70 S6 kinase and rapamycin sensitivity in human colorectal cancer. *Cancer Lett* **251:** 105-113.

Olson MF, Ashworth A, Hall A (1995) An essential role for Rho, Rac and Cdc42 GTPases in cell cycle progression through G1. *Science* **269:** 1270-1272.

Pantaloni D, Le Clainche C, Carlier MF (2001). Mechanism of actin-based motility. *Science* **292:** 1502-1506.

Pawlak G, Helfman DM (2001). Cytoskeletal changes in cell transformation and

tumorigenesis. *Curr Opin Genet Dev* **11:** 41-47.

Philp AJ, Campbell IG, Leet C, Vincan E, Rockman SP, Whitehead RH *et al* (2001). The phosphatidylinositol 3 '-kinase p85 alpha gene is an oncogene in human ovarian and colon tumors. *Cancer Res* **61:** 7426-7429.

Pon YL, Zhou HY, Cheung ANY, Ngan HYS, Wong AST (2008). p70 S6 kinase promotes epithelial to mesenchymal transition through Snail induction in ovarian cancer cells. *Cancer Res* **68:** 6524-6532.

Raftopoulou M, Hall A (2004). Cell migration: Rho GTPases lead the way. *Dev Biol* **265:** 23-32.

Ridley AJ, Schwartz MA, Burridge K, Firtel RA, Ginsberg MH, Borisy G *et al* (2003). Cell migration: Integrating signals from front to back. *Science* **302:** 1704-1709.

Sahin F, Kannangai R, Adegbola O, Wang JZ, Su G, Torbenson M (2004). mTOR and P70S6 kinase expression in primary liver neoplasms. *Clin Cancer Res* **10:** 8421-8425.

Sander EE, van Delft S, ten Klooster JP, Reid T, van der Kammen RA, Michiels F *et al* (1998). Matrix-dependent Tiam1/Rac signaling in epithelial cells promotes either cell-cell adhesion or cell migration and is regulated by phosphatidylinositol 3-kinase. *J Cell Biol* **143:** 1385-1398.

Sawada K, Radjabi AR, Shinomiya N, Kistner E, Kenny H, Becker AR *et al* (2007).

c-Met overexpression is a prognostic factor in ovarian cancer and an effective target for inhibition of peritoneal dissemination and invasion. *Cancer Res* **67:** 1670-1679.

Schmidt A, Bickle M, Beck T, Hall MN (1997). The yeast phosphatidylinositol kinase homolog TOR2 activates RHO1 and RHO2 via the exchange factor ROM2. *Cell* **88:** 531-542.

Schraml P, Schwerdtfeger G, Burkhalter F, Raggi A, Schmidt D, Ruffalo T *et al* (2003). Combined array comparative genomic hybridization and tissue microarray analysis suggest PAK1 at 11q13.5-q14 as a critical oncogene target in ovarian carcinoma. *Am J Pathol* **163:** 985-992.

Shayesteh L, Lu YL, Kuo WL, Baldocchi R, Godfrey T, Collins C *et al* (1999). PIK3CA is implicated as an oncogene in ovarian cancer. *Nat Genet* **21:** 99-102.

Siu MK, Wong ES, Chan HY, Kong DS, Woo NW, Tam KF *et al* (2009). Differential expression and phosphorylation of Pak1 and Pak2 in ovarian cancer: effects on prognosis and cell invasion. *Int J Cancer* **127:** 21-31.

Sowter HM, Corps AN, Smith SK (1999). Hepatocyte growth factor (HGF) in ovarian epithelial tumour fluids stimulates the migration of ovarian carcinoma cells. *Int J Cancer* **83:** 476-480.

Takaishi K, Sasaki T, Kotani H, Nishioka H, Takai Y (1997). Regulation of cell-cell

adhesion by Rac and Rho small G proteins in MDCK cells. *J Cell Biol* **139:** 1047-1059.

Theriault BL, Shepherd TG, Mujoomdar ML, Nachtigal MW (2007) BMP4 induces EMT and Rho GTPase activation in human ovarian cancer cells. *Carcinogenesis* **28:** 1153-1162.

Wong AS, Kim SO, Leung PC, Auersperg N, Pelech SL (2001) Profiling of protein kinases in the neoplastic transformation of human ovarian surface epithelium. *Gynecol Oncol* **82:** 305-311.

Wong AST, Roskelley CD, Pelech S, Miller D, Leung PCK, Auersperg N (2004). Progressive changes in Met-dependent signaling in a human ovarian surface epithelial model of malignant transformation. *Exp Cell Res* **299:** 248-256.

Zhou HY, Wong AST (2006). Activation of p70(S6K) induces expression of matrix metalloproteinase 9 associated with hepatocyte growth factor-mediated invasion in human ovarian cancer cells. *Endocrinology* **147:** 2557-2566.

Figure Legends

Figure 1 $p70^{S6K}$ activation induces reorganization of the actin cytoskeleton. (**a**) CaOV-3 and SKOV-3 cells were transfected with constitutively active $p70^{S6K}$ ($\Delta N_{54}\Delta C_{104}$ or $D_3E\text{-}E_{389}$). Cells were fixed and visualized by phase microscopy, or stained for F-actin using Texas red-conjugated phalloidin and observed by confocal microscopy. Whole cell lysates were analyzed for the levels of phosphorylated (p-) and total forms of S6 by Western blot analysis. (**b**) Cells were transfected with nonspecific (NS) or $p70^{S6K}$ siRNA or pretreated with rapamycin (Rp; 20 nM). Cells were then stimulated with HGF (10 ng/ml) for 1 h, fixed, and stained with Texas red-conjugated phalloidin. Expression of $p70^{S6K}$ was analyzed by Western blotting. β-actin was included as a loading control. Arrows indicate representative lamellipodia (↑) and filopodia (▲). Bar, 10 μm. Quantification of lamellipodia/filopodia is expressed as the mean number per 200 cells. Data are mean ± SD of three independent experiments. *, $P < 0.05$ compared with control or HGF and NS siRNA treated cells.

Figure 2 Directed cell migration is impaired in $p70^{S6K}$ knockdown cells. (**a**) Nonspecific (NS) or $p70^{S6K}$ siRNA cells were plated for the scrape-wound assay. Six hours after wounding, cells were fixed and stained with a Golgi marker (anti-GM130, red)

and nucleus (DAPI, blue). Percentage of cells exhibiting reoriented Golgi into the 120^{o} sector facing the wound was quantified. (**b**) Cells were seeded onto transwell inserts for cell migration assays. Quantification of migrated cells is expressed as the mean number per five fields. Experiments were repeated three times, and data are shown as mean ± SD. *, $P < 0.05$ compared with control or HGF and NS siRNA treated cells.

Figure 3 p70^{S6K} directly binds to actin. (**a**) CaOV-3 cell lysates were allowed to react with F-actin and then sedimented at 150,000 *g* (high speed). Equal amounts of pellets and supernatants were analyzed by SDS-PAGE and blotted with anti-phospho (p)-p70^{S6K}. (**b**) F-actin was incubated with different concentrations of purified active p70^{S6K} (0.05, 0.1, 0.2 μM) followed by high-speed cosedimentation. Equivalent samples of pellets and supernatants were resolved by SDS-PAGE and proteins were visualized by Coomassie Blue staining. (**c**) p70^{S6K} was mixed with F-actin buffer and centrifuged in either the presence (+) or absence (-) of F-actin. (**d**) Cells were treated with HGF (10 ng/ml) or transfected with constitutively active p70^{S6K} (D_3E-E_{389}) or (**e**) pretreated with cytochalasin D (Cyto D; 1 μM) for 30 min and then stimulated with HGF. Cells were fixed and stained with anti-p-p70^{S6K} (green), anti-myc (green), or phalloidin (red) and observed by confocal microscopy. Data shown represent three independent experiments

performed with similar results. Bar, 5 μm.

Figure 4 $p70^{S6K}$ cross-links and stabilzes F-actin. (**a**) CaOV-3 cell lysates were allowed to react with F-actin and sedimented at 14,000 *g*. Under this condition, the linear, unbundled F-actin is in the supernatant, whereas bundled F-actin sediment. Both pellet and supernatant were separated on SDS-PAGE and analyzed by Western blotting with anti-p-$p70^{S6K}$. (**b**) F-actin (4.5 μM) was incubated with increasing concentrations of $p70^{S6K}$ (0.05, 0.1 μM) and actin cross-linking assays were performed. (**c**) F-actin (2.5 μM) alone (○) or incubated with increasing concentrations of $p70^{S6K}$ (■ 0.05 μM; ▲ 0.1 μM) was monitored at 405 nm. (**d**) Negatively stained electron micrographs of F-actin in the absence or presence of 0.1 μM purified $p70^{S6K}$. Bar, 0.2 μm.

Figure 5 $p70^{S6K}$ inhibits cofilin-induced actin depolymerization. (**a**) G-actin (2.5 μM, 10% pyrene-labeled) was polymerized with the addition of actin polymerization buffer in the presence or absence of $p70^{S6K}$ (0.1 μM). (**b**) Pyrene-labeled actin filament disassembly was induced by addition of 1 μM recombinant purified human cofilin with or without 0.1 μM purified $p70^{S6K}$.

Figure 6 Specific activation of $p70^{S6K}$ on Rac1 and Cdc42, but not RhoA. (**a**) CaOV-3 cells were stimulated with HGF (10 ng/ml) for the indicated times (in minutes) or transfected with constitutively active $p70^{S6K}$ (D_3E-E_{389}). (**b**) In some cases, cells were transfected with nonspecific (NS) or $p70^{S6K}$ siRNA or (**c**) treated with rapamycin (Rp) before HGF stimulation. Lysates were analyzed for GTPase activation using pull-down assays as described in Materials and methods. GTP-bound (active) Rac1, Cdc42, and RhoA were examined by Western blotting. Alternatively, lysates were resolved in SDS-PAGE and blotted with anti-phospho (p)-$p70^{S6K}$, total $p70^{S6K}$, and Rac1, Cdc42 and RhoA. GTPγS served as a positive control and GDP was a negative control. The blots represent three independent experiments performed with similar results.

Figure 7 Rac1 and Cdc42 mediate $p70^{S6K}$-induced actin reorganization. (**a**) CaOV-3 cells were cotransfected with GFP-tagged constitutively active $p70^{S6K}$ (D_3E-E_{389}) and dominant negative Rac1 (N17Rac1) or Cdc42 (N17Cdc42) or (**b**) constitutively active Rac1 (L6Rac1) or Cdc42 (V12Cdc42). F-actin was visualized with Texas Red phalloidin. (**c**) Cells were treated with HGF (10 ng/ml), fixed, and stained with anti-p-$p70^{S6K}$ (green) or anti-Rac1/Cdc42 (red) Bar, 5 μm. Quantification of lamellipodia/filopodia is expressed as the mean number per 200 cells of three independent experiments. *, $P < 0.05$

compared with cells expressing D_3E-E_{389} or control cells.

Figure 8 PAK1 is required for $p70^{S6K}$ function. (**a**) CaOV-3 cells were transfected with constitutively active $p70^{S6K}$ (D_3E-E_{389}) (*left*), nonspecific (NS) siRNA, or $p70^{S6K}$ siRNA before HGF stimulation (10 ng/ml) (*right*). Lysates were analyzed by Western blot using anti-phospho-PAKs. (**b**) Cells were cotransfected with GFP-tagged D_3E-E_{389} and NS siRNA or PAK1 siRNA. F-actin was visualized with Texas Red phalloidin. Bar, 5 μm. Quantification of lamellipodia/filopodia is expressed as the mean number per 200 cells. (**c**) Cells were cotransfected with D_3E-E_{389} and dominant negative Rac1 (N17Rac1), Cdc42 (N17Cdc42), NS siRNA, or PAK1 siRNA. Transfected cells were seeded onto transwell inserts for cell migration assays. Quantification of migrated cells is expressed as the mean number per five fields. Data are mean ± SD of three independent experiments. *, $P < 0.05$ compared with cells expressing D_3E-E_{389}.

Figure 9 A model proposed to illustrate $p70^{S6K}$ in actin cytoskeleton reorganization and migration. $p70^{S6K}$ directly and indirectly reorganizes the actin cytoskeleton through cross-linking and stabilizing filaments and Rac1- and Cdc42-activating activities, which eventually leading to polarized actin structure and directed cell migration.

Supplementary Figure Legends

Figure 1 Effects of HGF and constitutive activation of $p70^{S6K}$ on cell proliferation. Control, HGF-treated (10 ng/ml), vector, or constitutively active $p70^{S6K}$ (D_3E-E_{389})-transfected cells cultured for 24 h were collected for MTT assay. A tetrazolium dye (MTT) [3-(4,5-dimethylthiazol-2-y1)-2,5-diphenyltetrazolium bromide] was added to a final concentration of 1 mg/ml, and plates were incubated for 4 h. The conversion of MTT to formazan was monitored by the absorbance of each well at 570 nm with 630 as the reference wavelength. The absorbance of control cells was arbitrarily set as 1, and cell growth was expressed as the fold changes compared with the control. Experiments were repeated three times, and data are shown as mean ± SD.

Figure 2 $p70^{S6K}$ binds actin and promotes Rac1 and Cdc42 activation in SKOV-3 cells. (**a**) Cells were transfected with myc-tagged constitutively active $p70^{S6K}$ (D_3E-E_{389}), stained with phalloidin (red) or anti-myc (green), and observed by confocal microscopy. Bar, 5 μm. Polymeric α-skeletal muscle actin was incubated with cell lysates for 30 min followed by (**b**) high-speed (150,000 *g*) or (**c**) low-speed (14,000 *g*) actin cosedimentation assays. Equal amounts of pellets and supernatants were detected by Western blotting with anti-phospho (p)-$p70^{S6K}$. (**d**) Cells were transfected with

nonspecific (NS) or $p70^{S6K}$ siRNA or (**c**) treated with rapamycin before HGF stimulation (10 ng/ml) and subjected to the pull-down assays. GST-bound (active) Rac1, Cdc42 and RhoA were analyzed by Western blot. GTPγS served as a positive control and GDP was a negative control.

Figure 3 Rho GTPases are not required for $p70^{S6K}$ activation. (**a**) CaOV-3 cells transfected with control or myc-tagged dominant negative Rac1 (N17Rac1), Cdc42 (N17Cdc42), or RhoA (N19RhoA) were analyzed by Western blotting after stimulation with HGF (10 ng/ml) for 1 h. (**b**) Lysates from CaOV-3 cells expressing control or constitutively active Rac1 (L61Rac1), Cdc42 (V12Cdc42), or RhoA (V14RhoA) were subjected to Western blotting. Membranes were probed initially for phospho (p)-$p70^{S6K}$, followed by stripping and reprobing with antibodies to $p70^{S6K}$. β-actin was included as a loading control. Exogenously expressed myc-tagged Rac, Cdc42, and Rho proteins were detected using a myc antibody.

Figure 4 Effect of $p70^{S6K}$ activation on the actin cytoskeleton of normal OSE. (**a**) OSE -529, OSE-545, and OSE-547 cells were transfected with myc-tagged constitutively active $p70^{S6K}$ (D_3E-E_{389}). Cells were fixed and visualized by phase microscopy, or (**b**)

stained for F-actin with Texas red-conjugated phalloidin (red) or D_3E-E_{389} with anti-myc (green) and observed by confocal microscopy. Bar, 5 μm.

Figure 5 $p70^{S6K}$ binds to and cross-links F-actin and regulates actin organization in HepG2 cells. (**a**) Cells were transfected with constitutively active $p70^{S6K}$ (D_3E-E_{389}), stained with phalloidin, and observed by confocal microscopy. Bar, 5 μm. Polymeric α-skeletal muscle actin was incubated with cell lysates for 30 min followed by (**b**) high-speed (150,000 *g*) or (**c**) low-speed (14,000 *g*) actin cosedimentation assays. Equal amounts of pellets and supernatants were detected by Western blotting with anti-phospho (p)-$p70^{S6K}$. (**d**) Cells were cotransfected with D_3E-E_{389} and dominant negative Rac1 (N17Rac1) or Cdc42 (N17Cdc42). F-actin was visualized with Texas Red phalloidin.

Figure 1

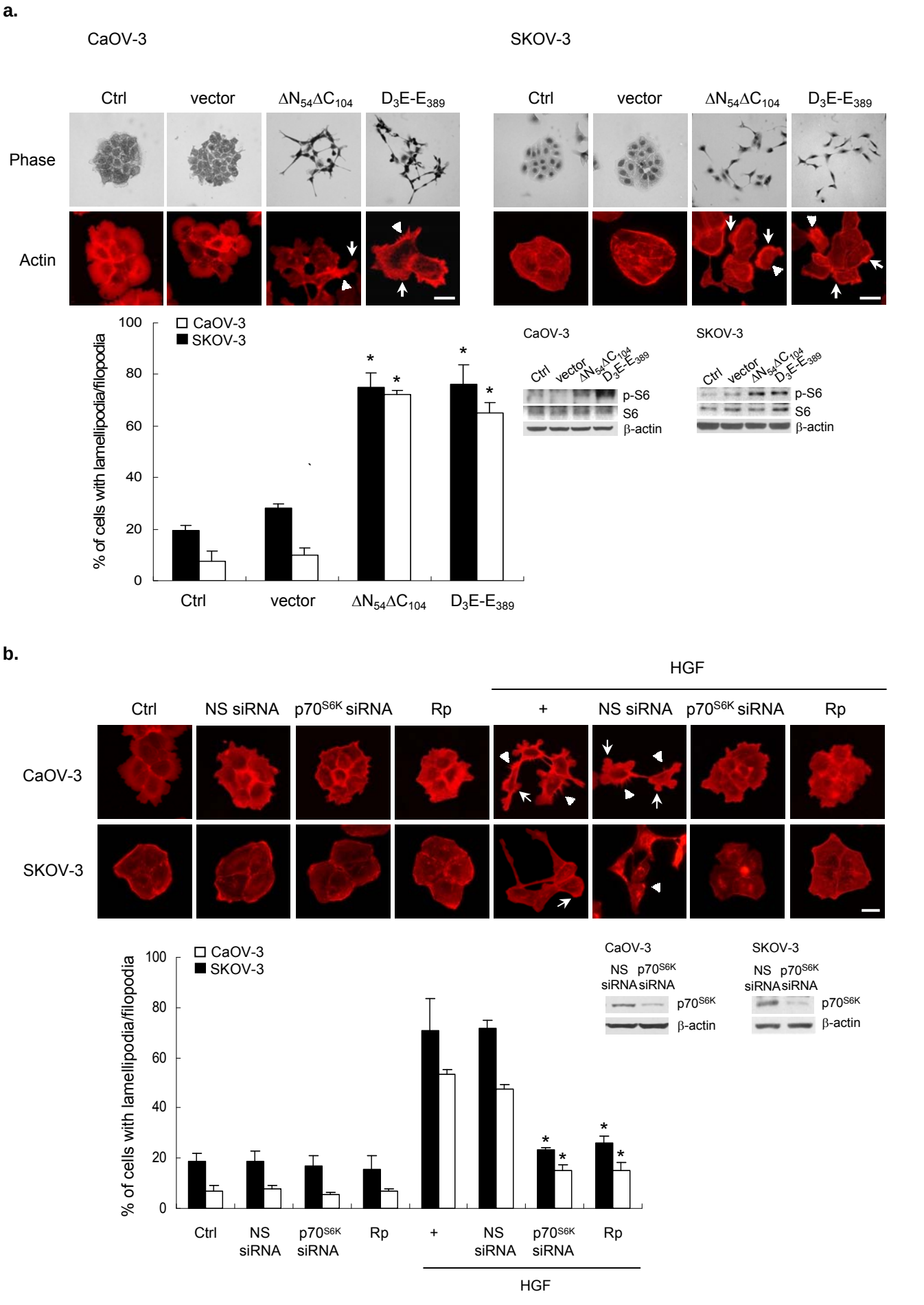
a.
CaOV-3
SKOV-3
Ctrl
vector
ΔN54ΔC104
D3E-E389
Phase
Actin
% of cells with lamellipodia/filopodia
CaOV-3
SKOV-3
p-S6
S6
β-actin
b.
HGF
NS siRNA
p70S6K siRNA
Rp
+
CaOV-3
SKOV-3

Figure 2

a.

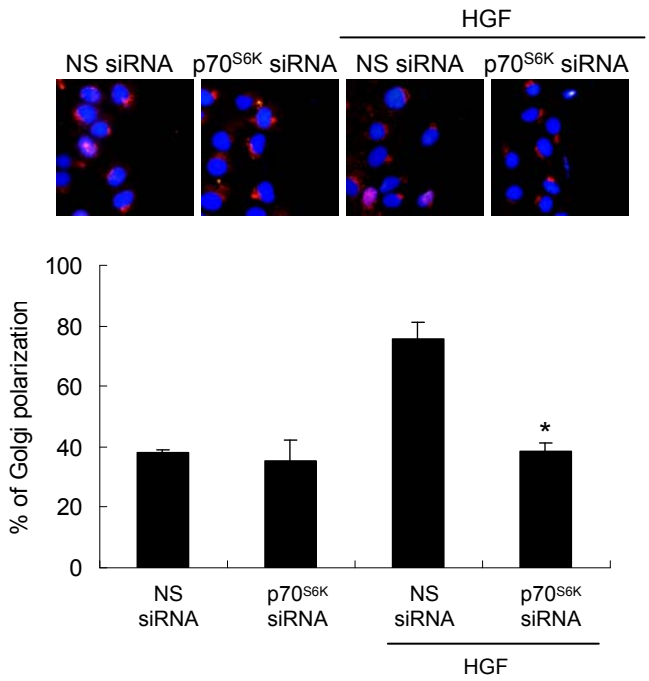
HGF
NS siRNA
p70S6K siRNA
NS siRNA
p70S6K siRNA
% of Golgi polarization
100
80
60
40
20
0
*
NS siRNA
p70S6K siRNA
NS siRNA
p70S6K siRNA
HGF

b.

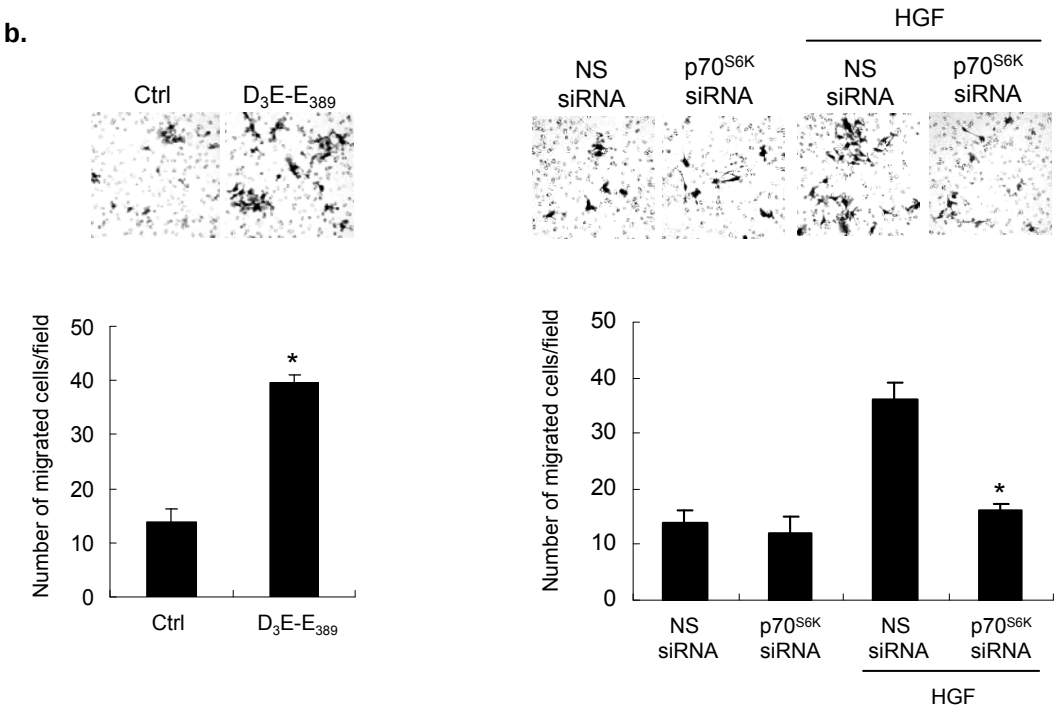
Ctrl
D3E-E389
Number of migrated cells/field
50
40
30
20
10
0
*
Ctrl
D3E-E389
HGF
NS siRNA
p70S6K siRNA
NS siRNA
p70S6K siRNA
Number of migrated cells/field
50
40
30
20
10
0
*
NS siRNA
p70S6K siRNA
NS siRNA
p70S6K siRNA
HGF

Figure 3

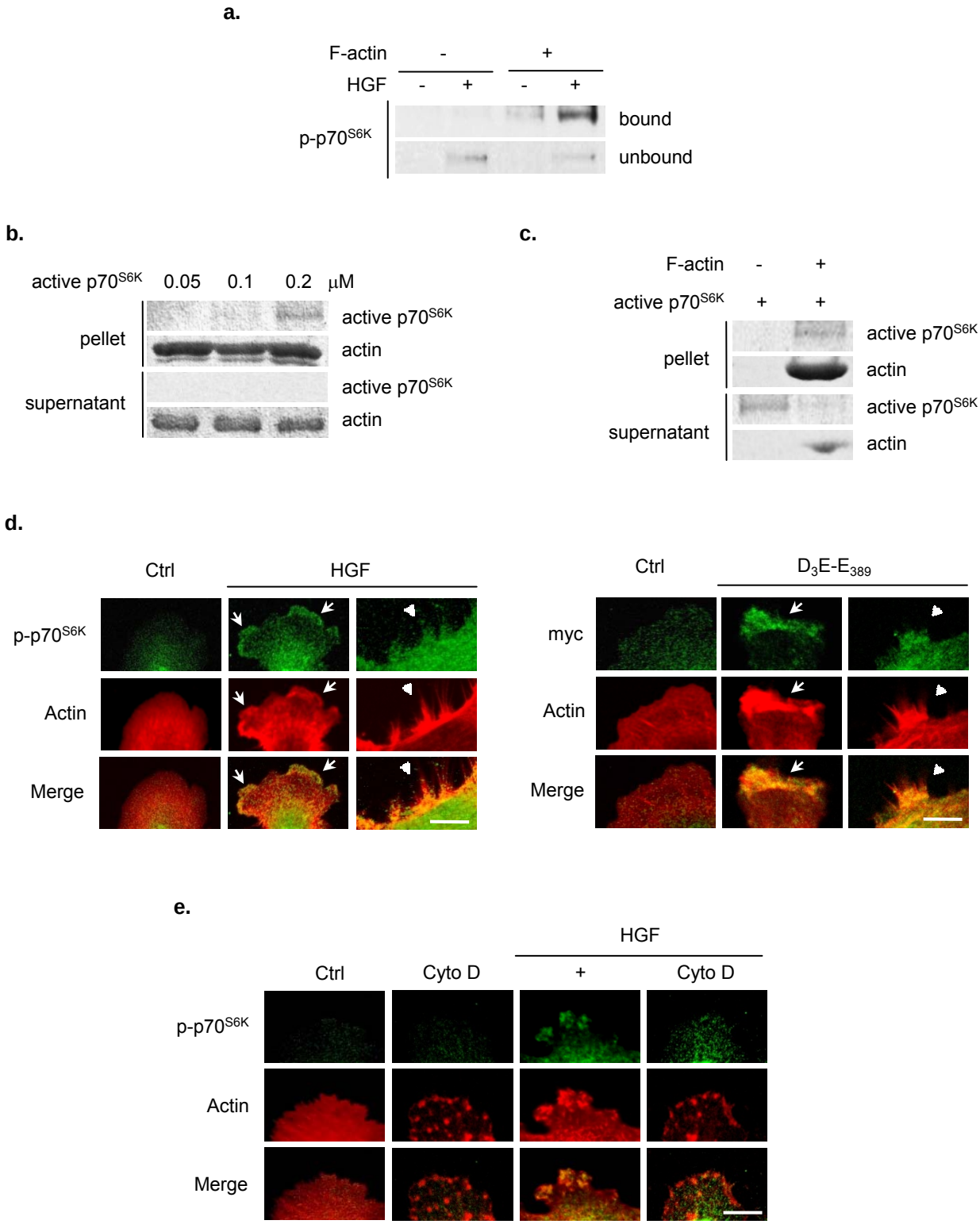
a.
F-actin - +
HGF - + - +
p-p70S6K
bound
unbound
b.
active p70S6K 0.05 0.1 0.2 μM
pellet
active p70S6K
actin
supernatant
active p70S6K
actin
c.
F-actin - +
active p70S6K + +
pellet
active p70S6K
actin
supernatant
active p70S6K
actin
d.
Ctrl
HGF
p-p70S6K
Actin
Merge
Ctrl
D3E-E389
myc
Actin
Merge
e.
HGF
Ctrl
Cyto D
+
Cyto D
p-p70S6K
Actin
Merge

a.

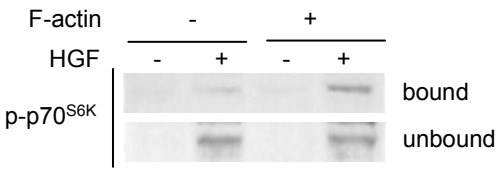
F-actin
-
+
HGF
-
+
-
+
p-p70S6K
bound
unbound

b.

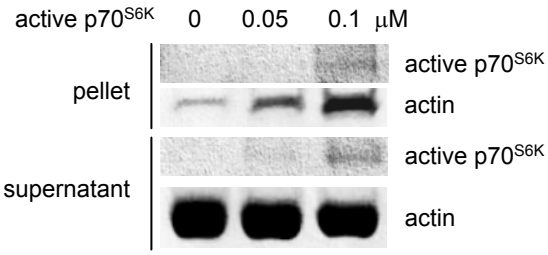
active p70S6K
0
0.05
0.1 μM
pellet
active p70S6K
actin
supernatant
active p70S6K
actin

c.

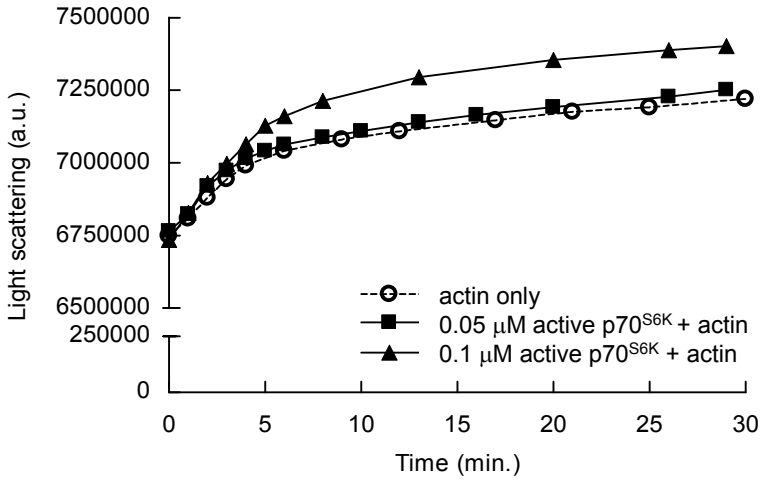
Light scattering (a.u.)
7500000
7250000
7000000
6750000
6500000
250000
0
0
5
10
15
20
25
30
Time (min.)
actin only
0.05 μM active p70S6K + actin
0.1 μM active p70S6K + actin

d.

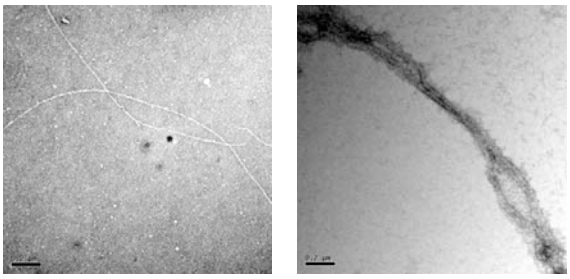

Figure 5

a.

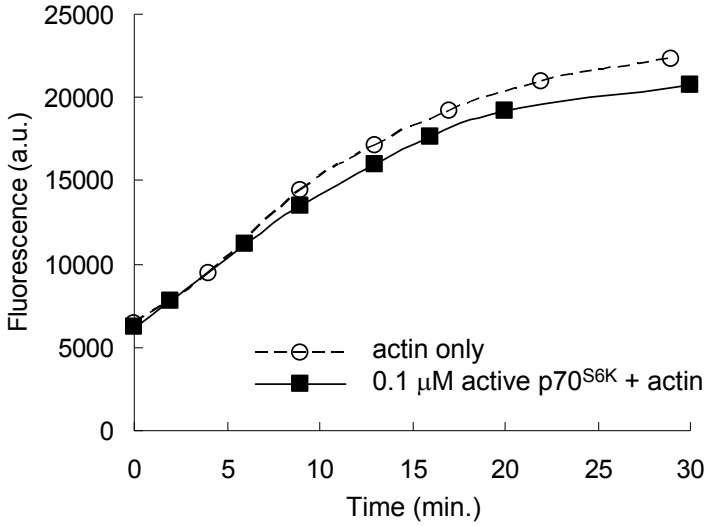
25000
20000
15000
10000
5000
0
Fluorescence (a.u.)
0
5
10
15
20
25
30
Time (min.)
actin only
0.1 μM active p70S6K + actin

b.

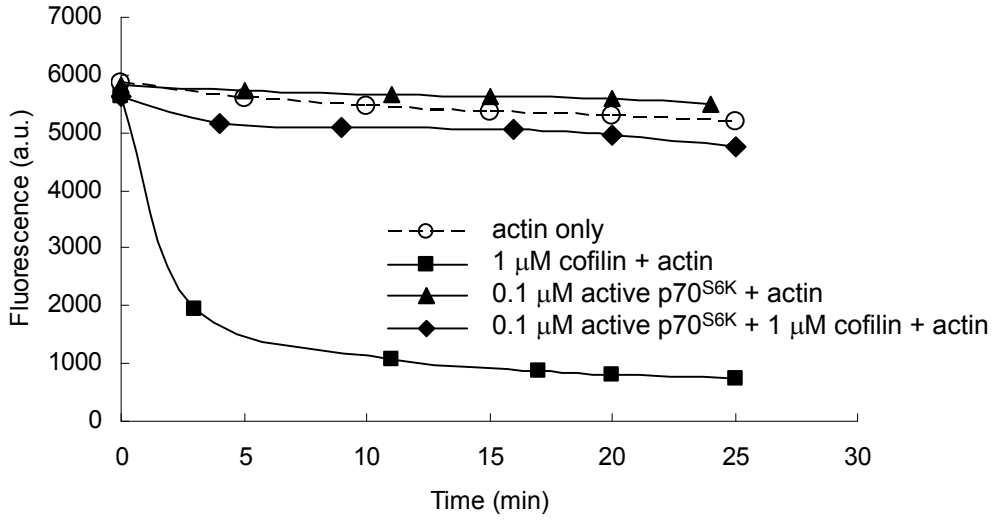
7000
6000
5000
4000
3000
2000
1000
0
Fluorescence (a.u.)
0
5
10
15
20
25
30
Time (min)
actin only
1 μM cofilin + actin
0.1 μM active p70S6K + actin
0.1 μM active p70S6K + 1 μM cofilin + actin

Figure 6

a.

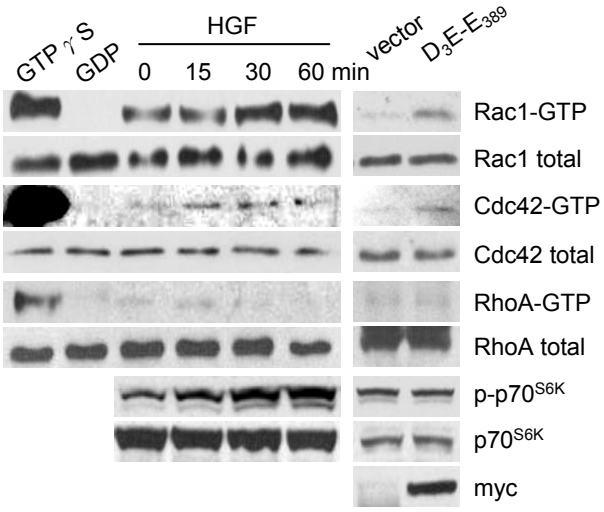
GTP γ S
GDP
HGF
0
15
30
60 min
vector
D3E-E389
Rac1-GTP
Rac1 total
Cdc42-GTP
Cdc42 total
RhoA-GTP
RhoA total
p-p70S6K
p70S6K
myc

b.

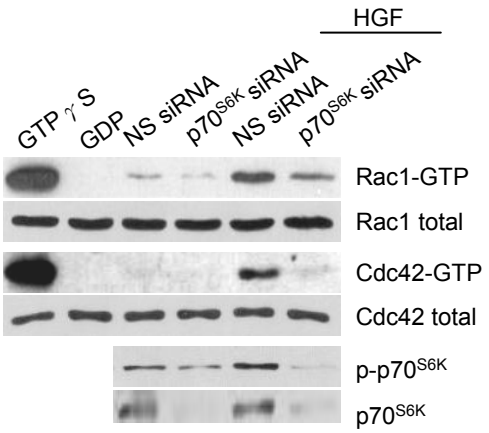
HGF
GTP γ S
GDP
NS siRNA
p70S6K siRNA
NS siRNA
p70S6K siRNA
Rac1-GTP
Rac1 total
Cdc42-GTP
Cdc42 total
p-p70S6K
p70S6K

c.

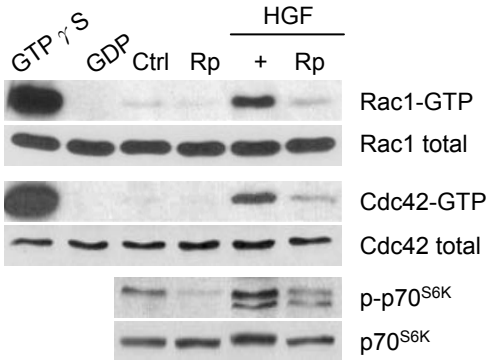
GTP γ S
GDP
Ctrl
Rp
HGF
+
Rp
Rac1-GTP
Rac1 total
Cdc42-GTP
Cdc42 total
p-p70S6K
p70S6K

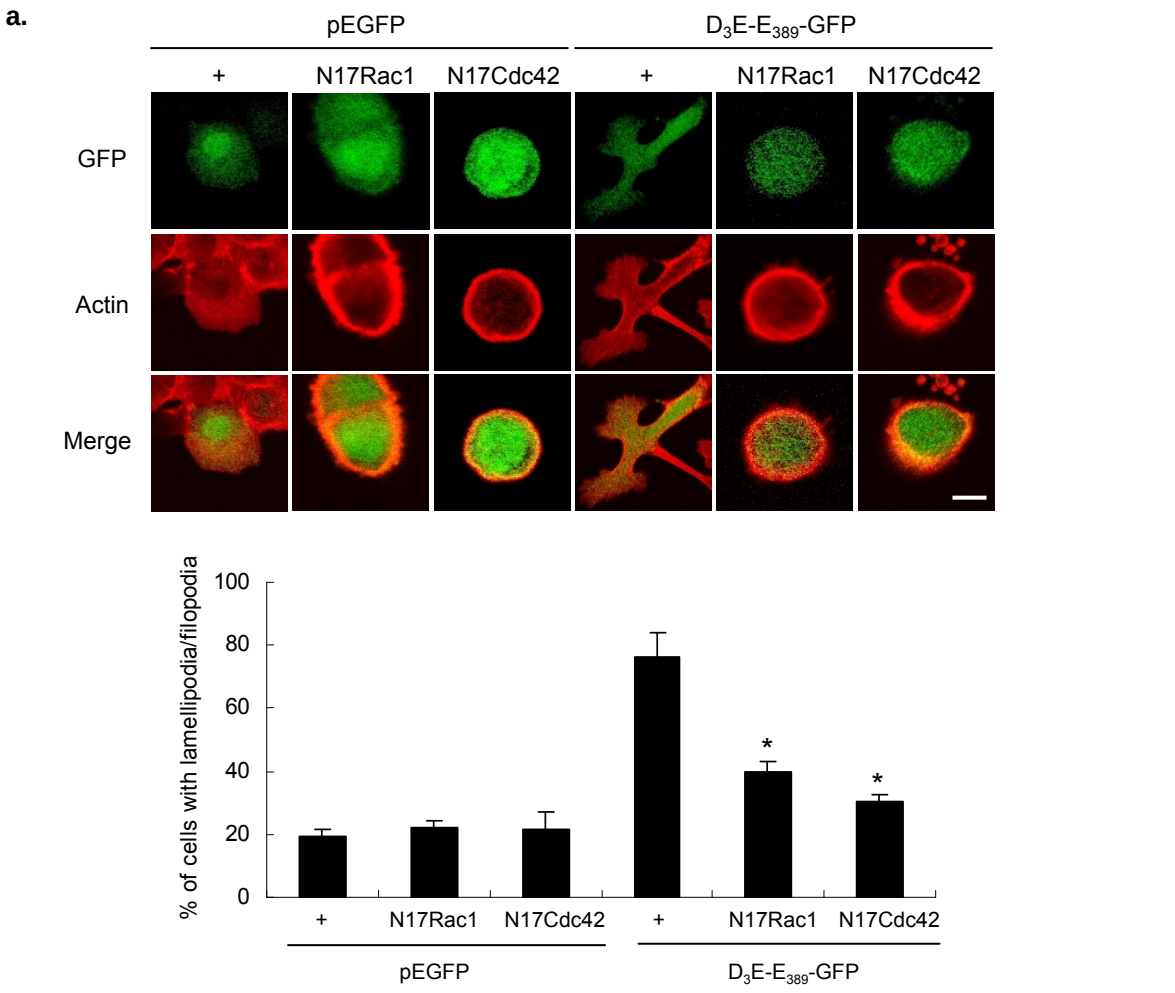
a.
pEGFP
D3E-E389-GFP
+
N17Rac1
N17Cdc42
+
N17Rac1
N17Cdc42
GFP
Actin
Merge
% of cells with lamellipodia/filopodia
100
80
60
40
20
0
*
*
+
N17Rac1
N17Cdc42
+
N17Rac1
N17Cdc42
pEGFP
D3E-E389-GFP

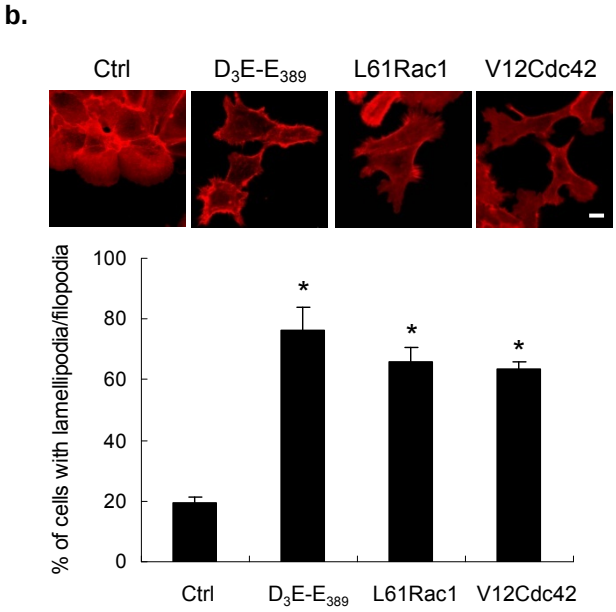
b.
Ctrl
D3E-E389
L61Rac1
V12Cdc42
% of cells with lamellipodia/filopodia
100
80
60
40
20
0
*
*
*
Ctrl
D3E-E389
L61Rac1
V12Cdc42

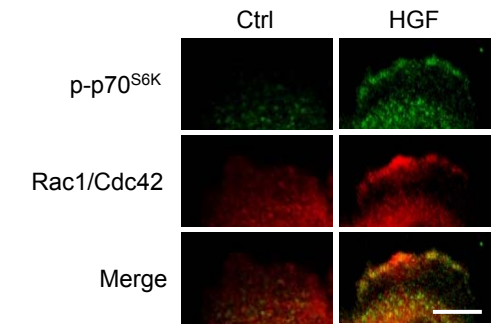
c.
Ctrl
HGF
p-p70S6K
Rac1/Cdc42
Merge

Figure 8

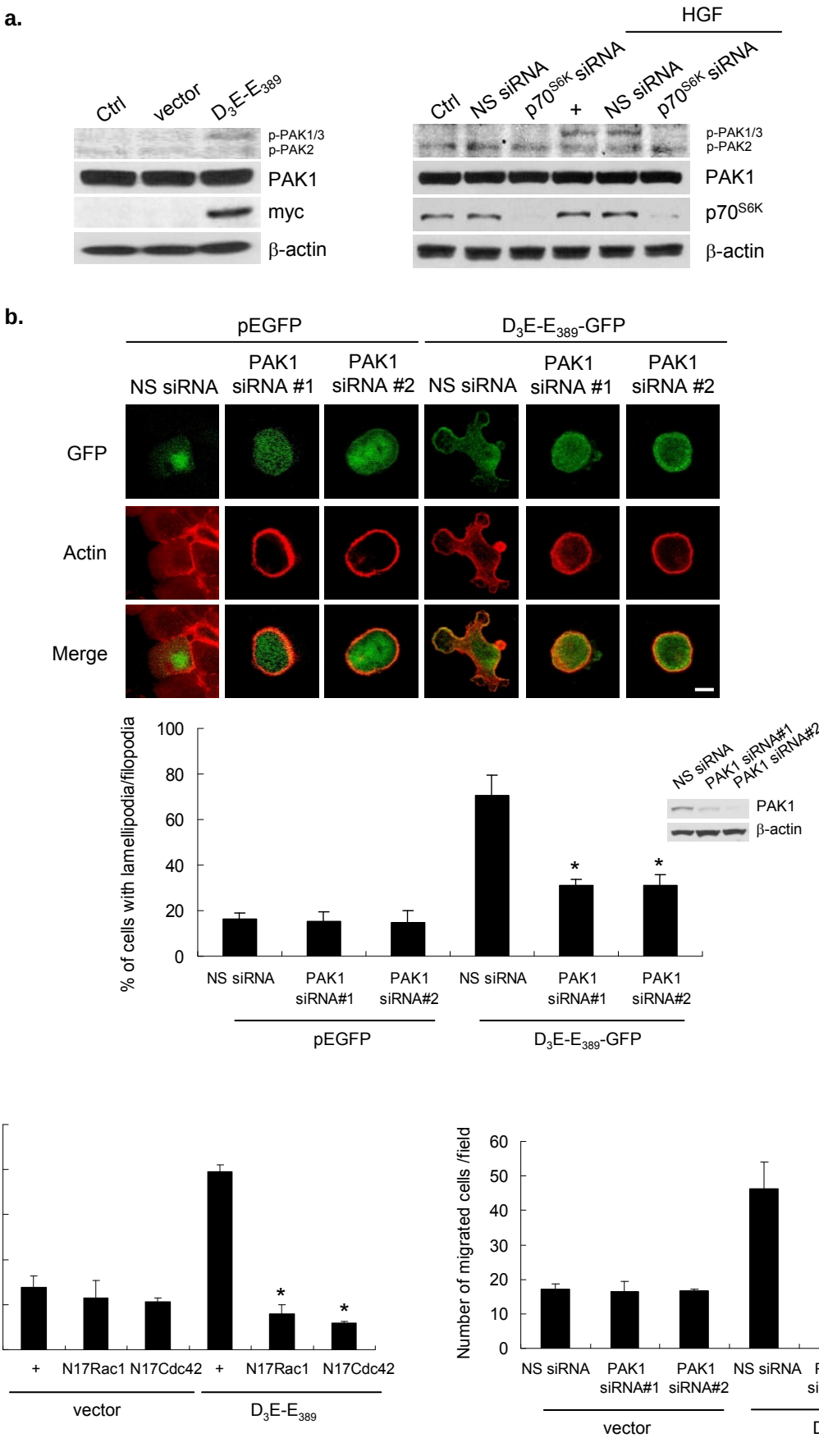
a.
HGF
Ctrl
vector
D3E-E389
Ctrl
NS siRNA
p70S6K siRNA
+
NS siRNA
p70S6K siRNA
p-PAK1/3
p-PAK2
PAK1
myc
β-actin
p70S6K
b.
pEGFP
D3E-E389-GFP
NS siRNA
PAK1 siRNA #1
PAK1 siRNA #2
GFP
Actin
Merge
% of cells with lamellipodia/filopodia
100
80
60
40
20
0
NS siRNA
PAK1 siRNA#1
PAK1 siRNA#2
pEGFP
D3E-E389-GFP
c.
Number of migrated cells/field
50
40
30
20
10
0
+
N17Rac1
N17Cdc42
vector
D3E-E389
Number of migrated cells /field
60
50
40
30
20
10
0
NS siRNA
PAK1 siRNA#1
PAK1 siRNA#2
vector
D3E-E389

Figure 9

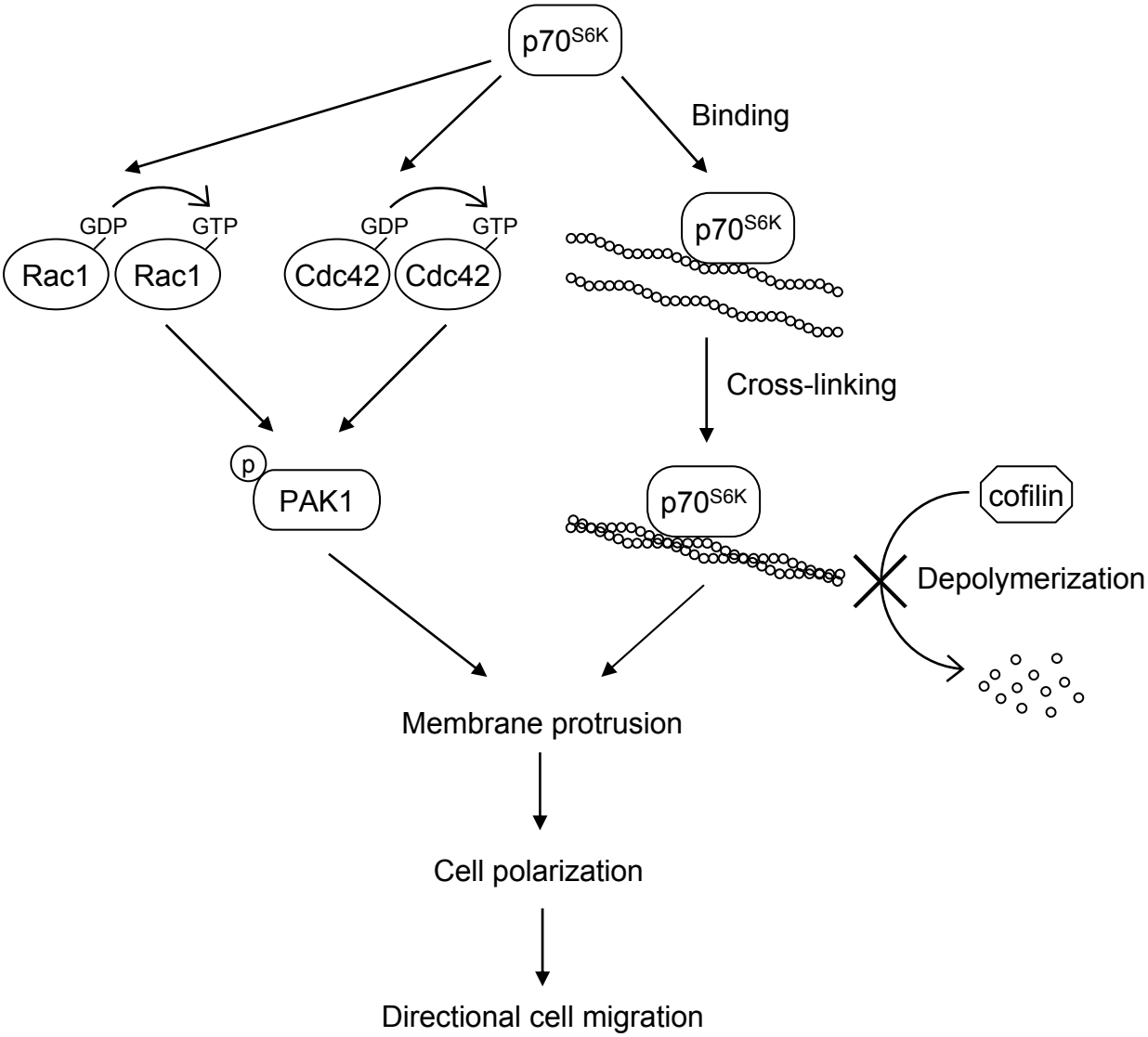
p70S6K
Binding
GDP
GTP
Rac1
Rac1
GDP
GTP
Cdc42
Cdc42
p70S6K
Cross-linking
p
PAK1
p70S6K
cofilin
Depolymerization
Membrane protrusion
Cell polarization
Directional cell migration

Supplementary Figure 1

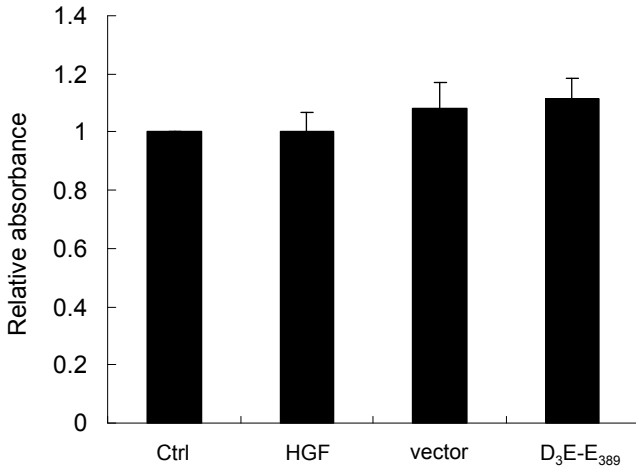

Supplementary Figure 2

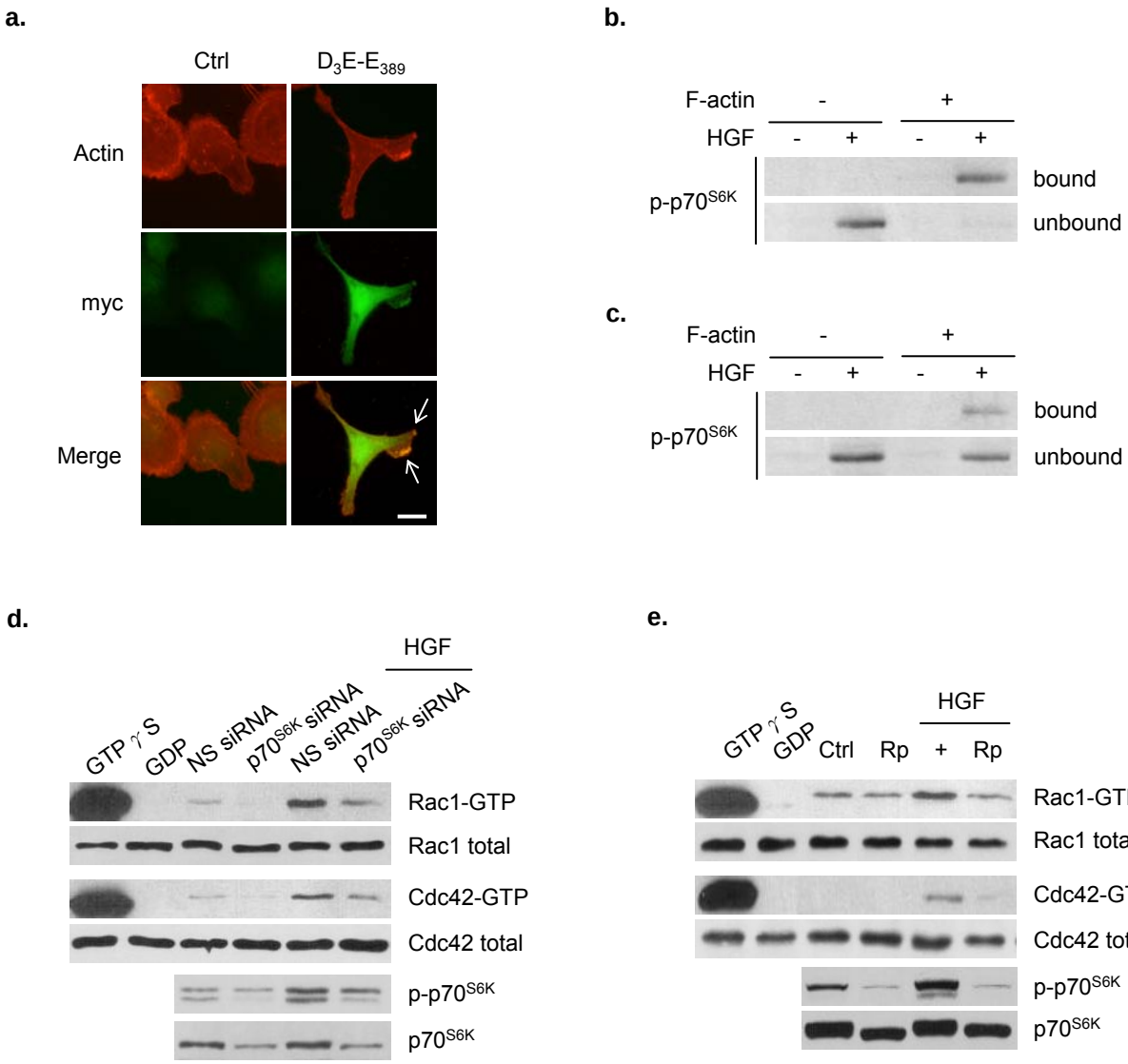

Supplementary Figure 3

a.

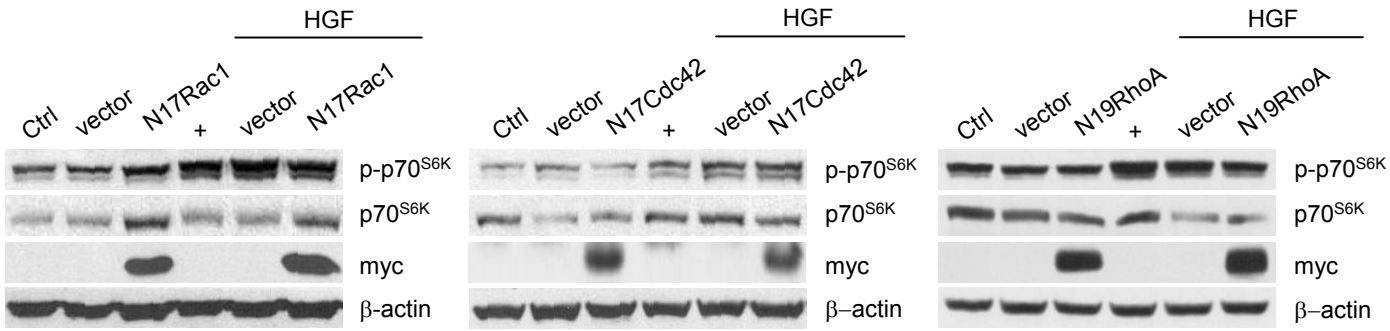

b.

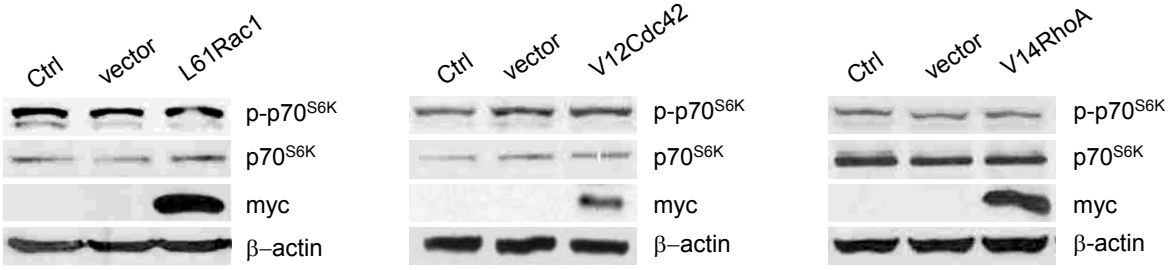

Supplementary Figure 4

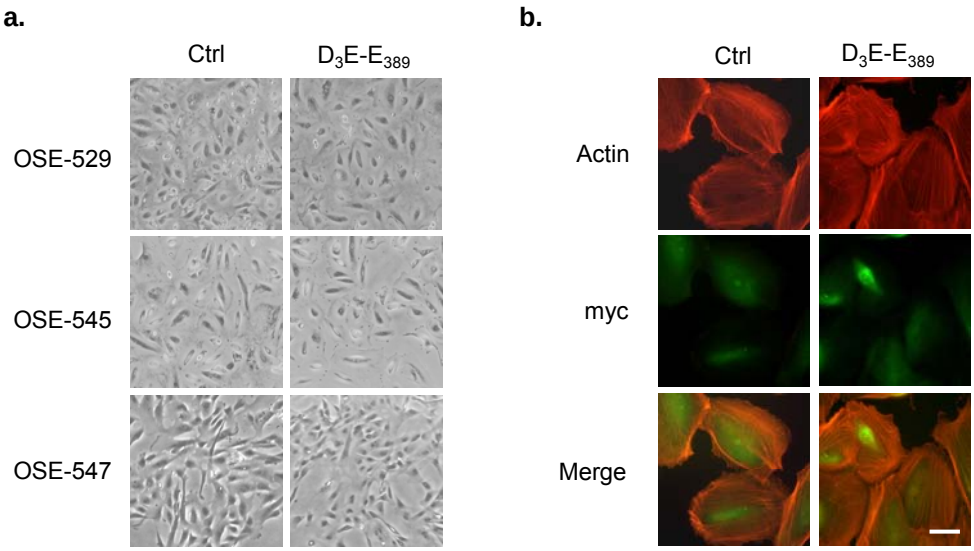

Supplementary Figure 5